Supporting Information

Solution and solid-state studies of hydrogen and halogen bonding with *N*-heterocyclic carbene supported nickel(II) fluoride complexes

Vargini G. Thangavadivale[a], Lukas Tendera[b], Rüdiger Bertermann[b], Udo Radius[b]*, Torsten Beweries[c]*, Robin N. Perutz[a]*

[a] *Department of Chemistry, University of York, Heslington, York, YO10 5DD, United Kingdom.*
[b] *Institut für Anorganische Chemie, Julius-Maximilians-Universität, Am Hubland, 97074 Würzburg, Germany.*
[c] *Leibniz-Institut für Katalyse, Albert-Einstein-Str. 29a, 18059 Rostock, Germany.*

Table of contents

Experimental details

General: All experiments involving oxygen and water sensitive materials were done under an argon or nitrogen atmosphere, in an argon filled glove box or standard Schlenk (10^{-2} mbar) techniques or high vacuum lines (10^{-4} mbar). General use solvents (AR grade) were dried over sodium, distilled, and stored under argon. Solvents such as hexane and THF were collected from a solvent purification system (removes oxygen and water) and were further dried and distilled. Deuterated solvents were dried over potassium and distilled prior to use. Normal laboratory nitrogen was dried further by passing through a column filled with activated molecular sieves.

NMR spectroscopy

NMR spectra were recorded on Bruker AMX500 and Bruker Avance NEO 400 spectrometers, unless otherwise stated, in tubes fitted with Young's PTFE stopcocks. All ^{1}H and ^{13}C chemical shifts are reported in ppm (δ) relative to tetramethylsilane and referenced using the chemical shifts of residual protio solvent resonances (benzene, δ 7.16), unless otherwise stated. The $^{31}P\{^{1}H\}$ NMR spectra were referenced to external H_3PO_4. The ^{19}F NMR spectra were referenced to external $CFCl_3$.

Solid-state NMR spectroscopy

Solid-state ^{19}F DP/MAS NMR spectra were recorded at 22 °C with a Bruker Avance NEO 400 NMR spectrometer with bottom layer rotors of ZrO_2 (open diameter 2.5 mm, Vespel bottom cap and Vespel rotor cap) containing approximately 11 µl of sample spinning the rotor at different speeds between 30 and 33.5 kHz (^{19}F, 376.50 MHz; DP = direct polarization, MAS = magic-angle spinning). All chemical shifts were calibrated by setting the ^{13}C low-field signal of adamantane to δ = 38.48 ppm by adjusting the field value of the spectrometer according to the IUPAC recommendations[1] with $\Xi[^{19}F]$ = 94.094011 MHz.[1] The components of the CSA tensor of the ^{19}F DP/MAS solid-state NMR spectra were simulated using the CSA model in the "Solid Lineshape Analysis"-Modul (2.2.4; 2013) integrated in the Bruker Biospin Software Topspin 4.1.4.

X-ray analysis

Crystals were immersed in a film of perfluoropolyether oil on a glass fiber MicroMount™ (MiTeGen) and transferred to a Rigaku XtaLAB Synergy-DW diffractometer with HyPix-6000HE detector and monochromated Cu-K_α or Mo-K_α radiation equipped with an Oxford Cryo 800 cooling unit. Data were collected at 100 K. The images were processed with the Crysalis software packages and equivalent reflections were merged. Corrections for Lorentz-polarization effects and absorption were performed if necessary and the structures were solved by direct methods. Subsequent difference Fourier syntheses revealed the positions of all other non-hydrogen atoms. The structures were solved by using the ShelXTL software package.[2] All non-hydrogen atoms were refined anisotropically. Hydrogen atoms were usually assigned to idealized positions and were included in structure factors calculations.

IR spectra

All infrared spectra were recorded on solid samples at room temperature on a Bruker Alpha FT-IR spectrometer using an ATR unit.

CHN analysis

Elemental analyses were performed in the microanalytical laboratory of the Institute of Inorganic Chemistry, Universität Würzburg, using an Elementar vario micro cube.

Synthesis of complexes and co-crystallisation experiments

Synthesis of trans-[Ni(F)(*i*Pr$_2$ Me$_2$Im)$_2$(C$_6$F$_5$)] (**2-*i*Pr$_2$Me$_2$Im**)

Hexafluorobenzene (35.6 μL, 57.0 mg; 306 μmol) was added to a solution of (*i*Pr$_2$Me$_2$Im)$_2$Ni(μ-C$_8$H$_{12}$)Ni(*i*Pr$_2$Me$_2$Im)$_2$[3] (145 mg, 153 μmol) in 7 mL of toluene and the reaction mixture was stirred for 24 h at room temperature. All volatiles were removed in vacuo and the remaining residue was suspended in 5 mL of hexane, collected by filtration and dried in vacuo to give **2-*i*PrMe$_2$Im** (78.0 mg, 129 μmol, 42 %) as a yellow powder. Yellow crystals suitable for single-crystal X-ray diffraction were obtained by storing a saturated solution in hexane at -30 °C.

^{1}H NMR (400.1 MHz, C$_6$D$_6$, 298 K): δ = 1.35 (d, 12H, $^3J_{HH}$ = 8.0 Hz, *i*Pr-C*H$_3$*), 1.56 (d, 12H, $^3J_{HH}$ = 8.0 Hz, *i*Pr-C*H$_3$*), 1.65 (s, 12H, NCC*H*$_3$CC*H*$_3$N), 7.16 (sept, 4H, *i*Pr-C*H*).

^{13}C{^{1}H} NMR (100.6 MHz, C$_6$D$_6$, 298 K): δ = 9.92 (NC*C*H$_3$C*C*H$_3$N), 21.6 (*i*Pr-*C*H$_3$), 22.6 (*i*Pr-*C*H$_3$), 53.4 (*i*Pr-*C*H), 124.5 (N*C*CH$_3$*C*CH$_3$N), 175.4 (d, *J* = 7.5 Hz, N*C*N).

^{19}F{^{1}H} NMR (376.5 MHz, C$_6$D$_6$, 298 K): δ = -115.87 (d, 2F, $^3J_{FF}$ = 27.0 Hz, aryl-*F$_{ortho}$*), -163.95 (t, 1F, $^3J_{FF}$ = 21.0 Hz, aryl-*F$_{para}$*), -165.55 (m, 2F, aryl-*F$_{meta}$*), -375.66 (s, 1F, Ni-*F*).

IR (ATR [cm^{-1}]): 2976 (w), 2939 (w), 2877 (vw), 1631 (vw), 1602 (vw), 1493 (s), 1469 (w), 1439 (s), 1426 (m), 1380 (s), 1367 (s), 1305 (m), 1274 (vw), 1222 (m), 1167 (vw), 1133 (w), 1108 (w), 1051 (m), 1041 (m), 1017 (w), 948 (vs), 907 (vw), 886 (vw), 774 (m), 712 (vw), 548 (vw), 506 (s), 478 (m), 418 (vw).

Elemental analysis C$_{28}$H$_{40}$F$_6$N$_4$Ni [605.34 g/mol] calculated (found): C 55.56 (55.66), H 6.66 (7.06), N 9.26 (9.34).

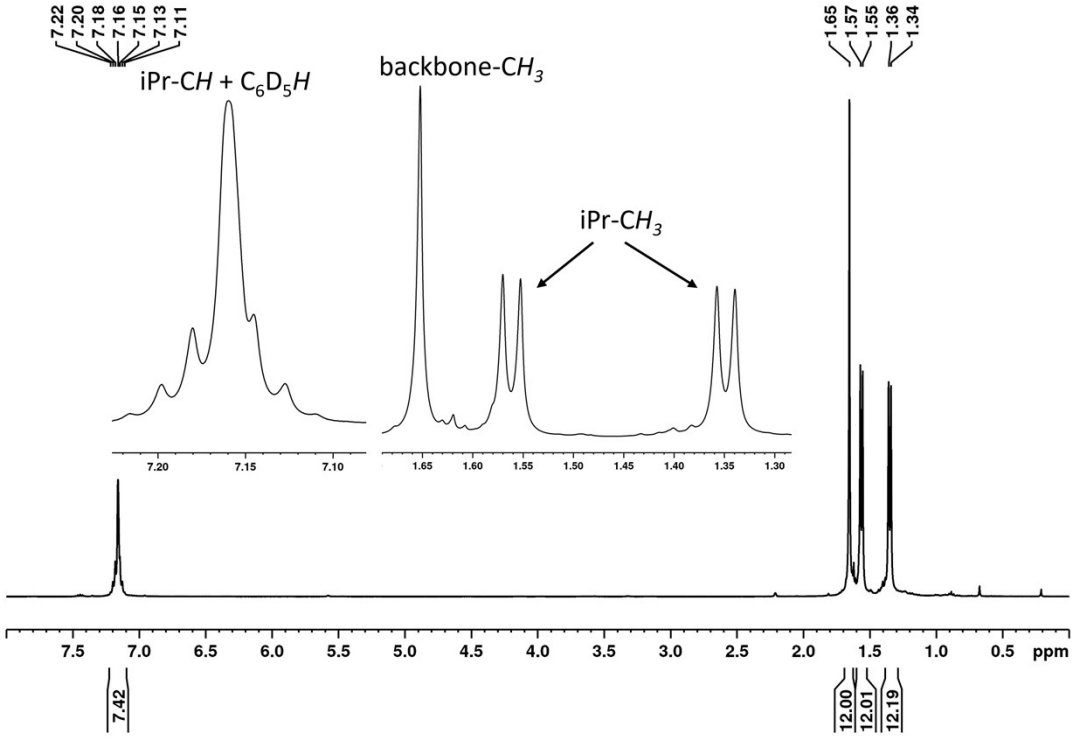

Figure S1. ^{1}H NMR spectrum of **2-*i*PrMe$_2$Im** (400.1 MHz, C$_6$D$_6$, 298 K).

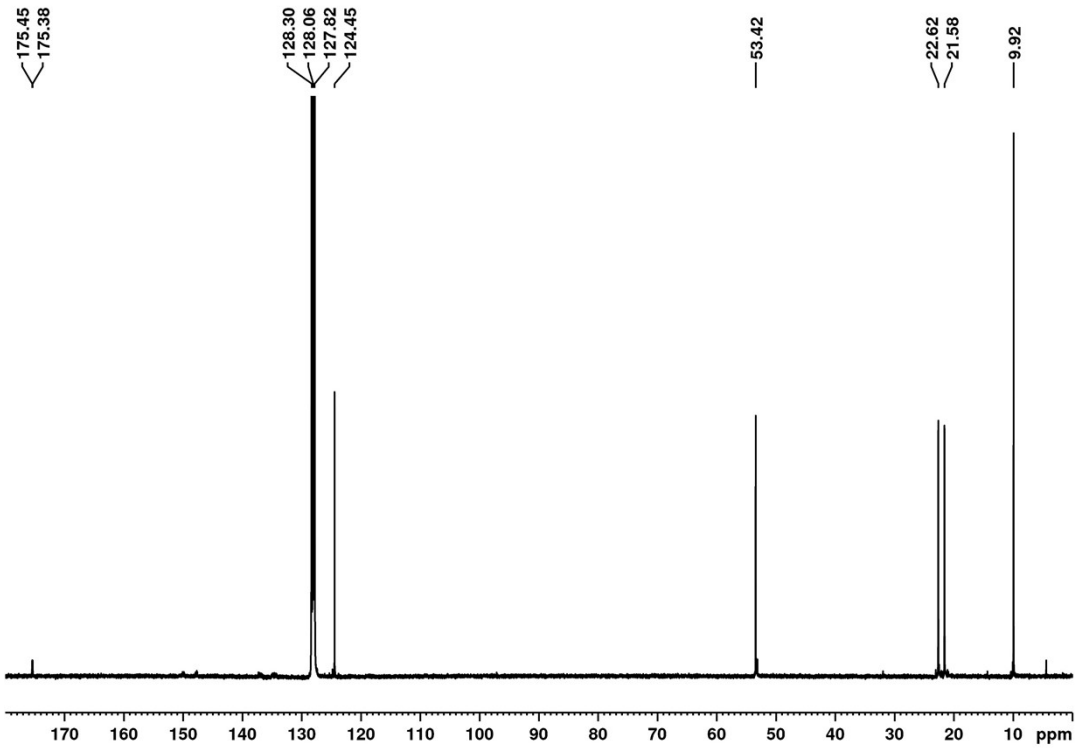

Figure S2. $^{13}C\{^{1}H\}$ NMR spectrum of **2-*i*PrMe$_2$Im** (100.6 MHz, C_6D_6, 298 K).

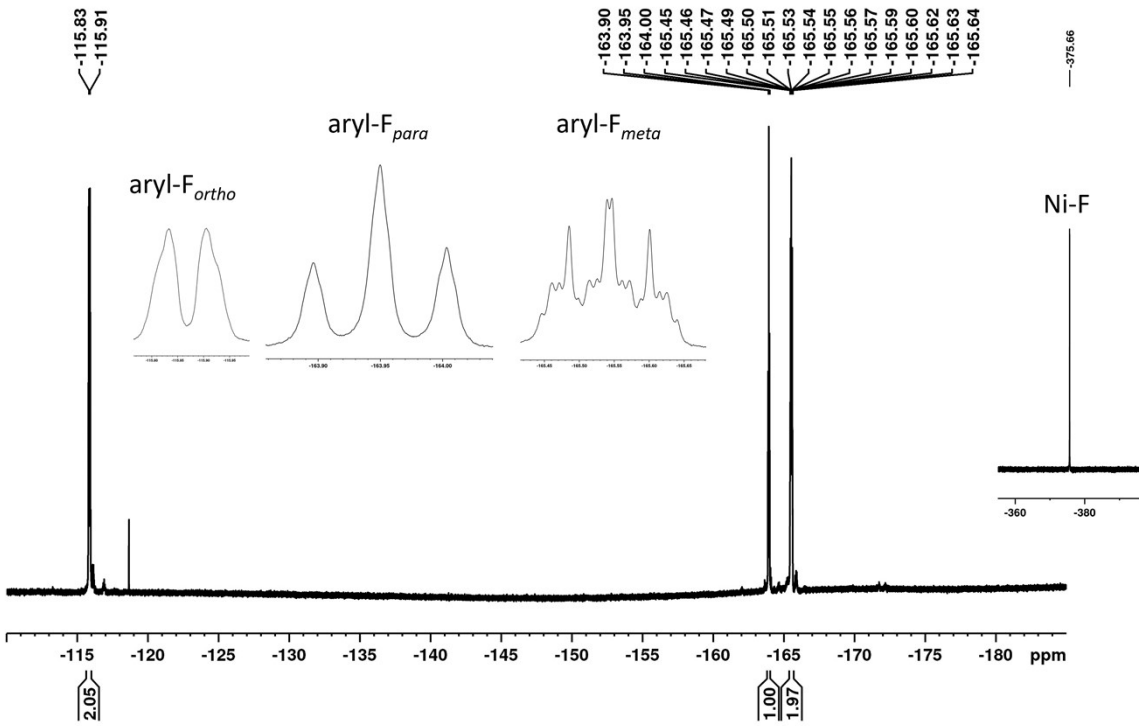

Figure S3. $^{19}F\{^{1}H\}$ NMR spectrum of **2-*i*PrMe$_2$Im** (376.5 MHz, C_6D_6, 298 K).

Synthesis of the adduct ***2-iPrMe$_2$Im•I-C$_6$F$_4$-I***

Complex **2-*i*PrMe$_2$Im** (25.0 mg, 41.3 μmol) and 1,4-$C_6F_4I_2$ (8.3 mg, 20.7 μmol) were dissolved in 1 mL of toluene. After storing the solution for 14 days at -30 °C crystals were formed that were isolated by decanting the solution (yield: 18.0 mg).

Synthesis of adduct ***2-iPrIm•I-C$_6$F$_4$-I****:*

Complex **2-iPrIm** (50.0 mg, 91.0 μmol) and $C_6F_4I_2$ (18.3 mg, 45.5 μmol) were dissolved in 1.5 mL of toluene. After storing the solution overnight at -30 °C crystals were formed that were isolated by decanting (yield: 36.0 mg).

NMR titration experiments

Preparation of stock solutions

It should be noted that concentration used for titration experiments were much lower compared to previous experiments with phosphine substituted nickel fluorides. When using the same concentrations as before, unreliable data were obtained due to very strong binding that caused very strong curvature of the titration curves already at very low guest-to-host ratios.

Table S1. Composition of the host and guest stock solutions.

	Host		**Guest**	
	Mass of host [mg]	Mass of solvent [mg]	Mass of guest [mg]	Mass of solvent [mg]
2-*i*PrIm/indole	8.1	5190.1	10.7	4926.5
2-*i*PrIm/C_6F_5I	39.6	4590.5	85.6	2919.0

Table S2. Mass of the host and guest stock solutions in NMR samples used for titration experiments.

2-*i*PrIm/C_6F_5I		**2-*i*PrIm/indole**	
Host [mg]	Guest [mg]	Host [mg]	Guest [mg]
331.93	0.00	400.42	0.00
337.21	19.88	395.69	16.38
327.46	40.55	394.19	25.38
339.04	49.64	393.84	34.95
332.51	59.86	393.15	50.53
338.70	74.35	393.26	57.79
336.18	88.73	394.07	69.56
332.85	97.94	396.61	81.21
337.89	127.36	396.84	90.21
338.47	166.34	397.07	105.32
341.45	207.67	395.92	171.65
341.33	242.26		
333.88	294.71		

General procedure for NMR titrations

The complex *trans*-Ni(F)(*i*Pr$_2$Im)$_2$(C_6F_5) (**2-*i*PrIm**) was prepared according to literature known procedure.[4] The stock solutions of host and guest were prepared by measuring the mass of the host, guest and the solvent added. The procedure for NMR spectroscopic titrations followed was similar to the previously reported titrations.[5] The samples for the titration were prepared in NMR tubes fitted with Young's caps inside the glove box, by measuring the exact mass of the host and the guest added. The solvent was added to make the total volume 6 mL. The samples were then allowed to thermostat in a cold bath which was approximately in the temperature required. The sample was allowed to stand inside the spectrometer for 2 minutes to allow the sample to attain the required temperature. The temperature of the NMR probe was corrected using a procedure described earlier.[6] All other temperatures were determined from a linear regression plot of set vs. calculated data.

Fitting of the titration data

The titration data obtained from the ^{19}F NMR spectra were used to fit the formation of a 1:1 adduct between the halogen or hydrogen bond donor and the nickel fluoride, as shown below.

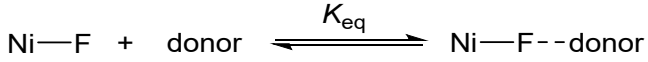

The downfield shift of the coordinated fluoride resonance from that of the free fluoride resonance ($\Delta\delta$ F) and the equilibrium constant associated with adduct formation are the two parameters fitted for the different temperatures. The two parameters were fitted with a Microsoft Excel macro program developed by Professor Christopher Hunter (University of Cambridge). From the equilibrium constants obtained at different temperatures, the van't Hoff plot was constructed which gave $\Delta H°$ and $\Delta S°$.

Summary of equilibrium constants

Table S3. Equilibrium constants and the downfield shift of the coordinated nickel fluoride resonance from that of the free fluoride resonance measured at various temperatures for adduct formation with indole in toluene.

Temperature [K]	**Equilibrium constant K_{eq} / 10^2**	$\Delta\delta$ **F [ppm]**
265.7	41.6	23.5
277.7	20.8	24.6
290.3	11.3	25.0
300.6	7.2	25.5
311.9	4.4	26.3
322.8	3.1	26.3

Table S4. Equilibrium constants and the downfield shift of the coordinated nickel fluoride resonance from that of the free fluoride resonance measured at various temperatures for adduct formation with C_6F_5I in toluene.

Temperature [K]	**Equilibrium constant K_{eq}**	$\Delta\delta$ **F [ppm]**
257.0	171.0	43.5
265.7	114.2	43.3
277.7	73.7	43.7
290.3	45.7	41.6
300.6	33.0	45.9
311.9	24.1	46.8

Table S5. Summary of titration data, hydrogen bonding of **2-*i*Pr$_2$Im** with indole in toluene.

entry	mass of host [mg]	mass of guest [mg]	molar ratio	Chemical shift δ(^{19}F) at temperature [ppm] 265.7 K	277.7 K	290.3 K	300.6 K	311.9 K	322.8 K
1	400.42	0.00	0.00	-370.93	-375.12	-374.98	-376.29	-377.30	-378.21
2	395.69	16.38	0.27	-365.08	-370.09	-371.13	-372.97	-374.73	-376.09
3	394.19	25.38	0.42	-361.73	-367.38	-368.77	-371.12	-373.20	-374.97
4	393.84	34.95	0.58	-358.93	-364.90	-366.72	-369.43	-371.79	-373.84
5	393.15	50.53	0.85	-355.84	-362.00	-364.21	-367.15	-369.85	-372.20
6	393.26	57.79	0.97	-354.57	-360.72	-363.03	-366.10	-368.95	-371.41
7	394.07	69.56	1.16	-353.17	-359.32	-361.70	-364.82	-367.79	-370.18
8	396.61	81.21	1.35	-352.00	-358.17	-360.56	-363.72	-366.83	-369.48
9	396.84	90.21	1.50	-351.32	-357.41	-359.78	-362.95	-366.14	-368.87
10	397.07	105.32	1.75	-350.38	-356.29	-358.54	-361.77	-364.85	-367.82
11	395.92	171.65	2.86	-347.93	-353.32	-355.16	-358.10	-361.17	-364.18

Table S6. Summary of titration data, halogen bonding of **2-*i*Pr$_2$Im** with C_6F_5I in toluene.

entry	mass of host [mg]	mass of guest [mg]	molar ratio	Chemical shift δ(^{19}F) at temperature [ppm] 257.0 K	265.7 K	277.7 K	290.3 K	300.6 K	311.9 K
1	331.93	0.00	0.00	-372.23	-373.34	-374.59	-374.63	-375.67	-376.59
2	337.21	19.88	0.37	-363.65	-366.57	-369.44	-370.83	-372.65	-374.12
3	327.46	40.55	0.79	-356.65	-360.56	-364.53	-366.99	-369.45	-371.69
4	339.04	49.64	0.93	-354.71	-358.77	-363.05	-365.83	-368.45	-370.75
5	332.51	59.86	1.14	-352.21	-356.63	-361.12	-364.27	-367.14	-369.74
6	338.70	74.35	1.39	-349.62	-354.19	-358.94	-362.41	-365.52	-368.24
7	336.18	88.73	1.68	-347.31	-352.02	-356.82	-360.74	-364.03	-366.97
8	332.85	97.94	1.87	-345.97	-350.81	-355.71	-359.62	-363.08	-366.14
9	337.89	127.36	2.39	-342.99	-347.73	-352.73	-356.83	-360.49	-363.99
10	338.47	166.34	3.12	-339.98	-344.32	-349.31	-353.58	-357.47	-361.05
11	341.45	207.67	3.86	-337.71	-341.98	-346.78	-351.04	-354.99	-358.95
12	341.33	242.26	4.51	-335.82	-340.11	-344.73	-348.97	-352.96	-356.79
13	333.88	294.71	5.61	-335.14	-338.87	-343.17	-346.84	-350.57	-354.48

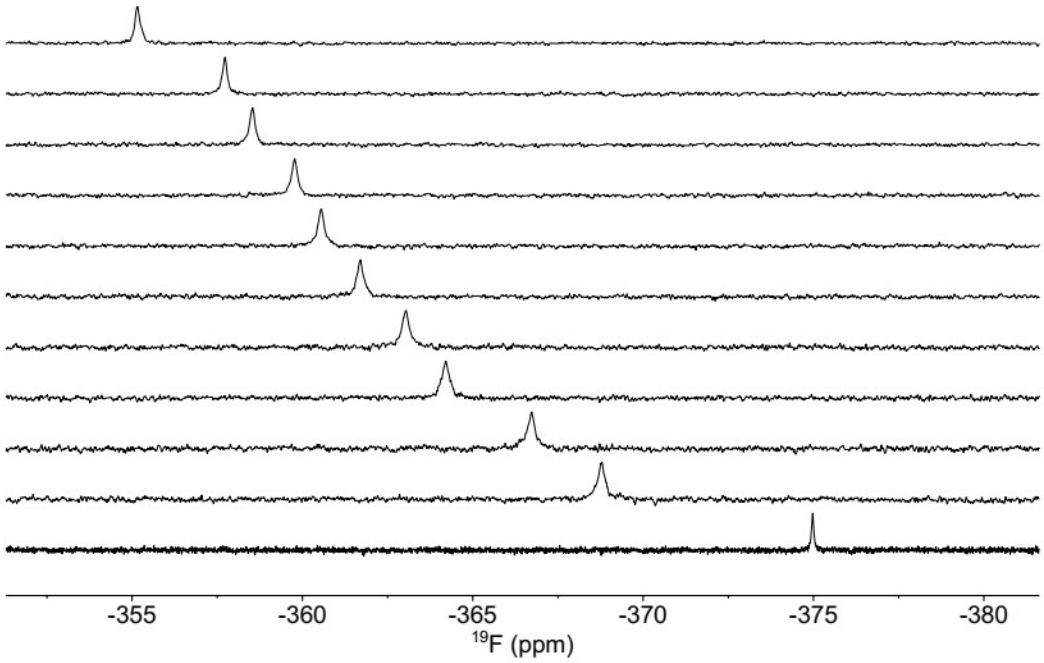

Figure S4. $^{19}F\{^{1}H\}$ NMR spectra of titration of **2-*i*PrMe$_2$Im** with C_6F_5I in toluene at 290.3 K, showing the downfield shift of the Ni-F resonance upon stepwise addition of halogen bond donor (bottom to top, 376.5 MHz, 298 K).

Crystallographic data

Table S7. Crystal data and structure refinement data.

	2-*i*Pr$_2$Im·C$_6$F$_4$I$_2$	**2-*i*Pr$_2$Me$_2$Im·C$_6$F$_4$I$_2$**	**2-*i*Pr$_2$Me$_2$Im**
Empirical formula	C44 H48 F10 I2 N4 Ni	C38 H48 F8 I N4 Ni	C31 H47 F6 N4 Ni
Formula weight	1135.37	898.41	648.43
Temperature	100(2) K	100.0(1) K	100.0(1) K
Wavelength	1.54184 Å	1.54184 Å	0.71073 Å
Crystal system	Triclinic	Triclinic	Triclinic
Space group	P-1	P-1	P-1
Unit cell dimensions	a = 17.5163(2) Å b = 18.1903(2) Å c = 18.3475(5) Å α= 104.496(1)° β= 113.590(1)° γ = 104.443(1)°	a = 10.5397(2) Å b = 10.7172(2) Å c = 19.4459(5) Å α= 105.371(2)° β= 98.187(2)° γ = 103.797(2)°	a = 11.3574(3) Å b = 11.4628(3) Å c = 12.8226(3) Å α= 102.524(2)° β= 91.226(2)° γ = 93.168(2)°
Volume	4767.32(10) Å^3	2006.65(8) Å^3	1626.18(7) Å^3
Z	4	2	2
Density (calculated)	1.582 Mg/m^3	1.487 Mg/m^3	1.324 mg/m^3
Absorption coefficient	11.396 mm^{-1}	7.334 mm^{-1}	0.657 mm^{-1}
F(000)	2256	914	686
Crystal size	0.380 x 0.100 x 0.050 mm^3	0.210 x 0.070 x 0.030 mm^3	0.331 x 0.150 x 0.124 mm^3
Theta range for data collection	2.730 to 78.219°	2.415 to 74.504°	2.163 to 26.372°
Index ranges	-22<=h<=22, -21<=k<=23, -23<=l<=19	-13<=h<=13, -13<=k<=13, -24<=l<=22	-14<=h<=14, -14<=k<=14, -16<=l<=16
Reflections collected	97369	40222	21609
Independent reflections	19945 [R(int) = 0.0589]	8175 [R(int) = 0.0480]	6645 [R(int) = 0.0341]
Completeness to theta = 26.000°	100.0 %	99.9 %	100.0 %
Absorption correction	Gaussian	Gaussian	Gaussian
Max. and min. transmission	1.000 and 0.073	1.000 and 0.315	1.000 and 0.395
Refinement method	Full-matrix least-squares on F^2	Full-matrix least-squares on F^2	Full-matrix least-squares on F^2
Data / restraints / parameters	19945 / 618 / 1189	8175 / 0 / 482	6645 / 0 / 392
Goodness-of-fit on F^2	1.079	1.102	1.056
Final R indices [I>2sigma(I)]	R1 = 0.0401, wR2 = 0.1102	R1 = 0.0303, wR2 = 0.0801	R1 = 0.0374, wR2 = 0.0970
R indices (all data)	R1 = 0.0440, wR2 = 0.1135	R1 = 0.0322, wR2 = 0.0815	R1 = 0.0434, wR2 = 0.1007
Extinction coefficient	n/a	n/a	n/a
Largest diff. peak and hole	2.234 and -1.167 e.Å^{-3}	1.258 and -1.333 e.Å^{-3}	1.224 and -0.461 e.Å^{-3}
CCDC	2214533	2214532	2214531

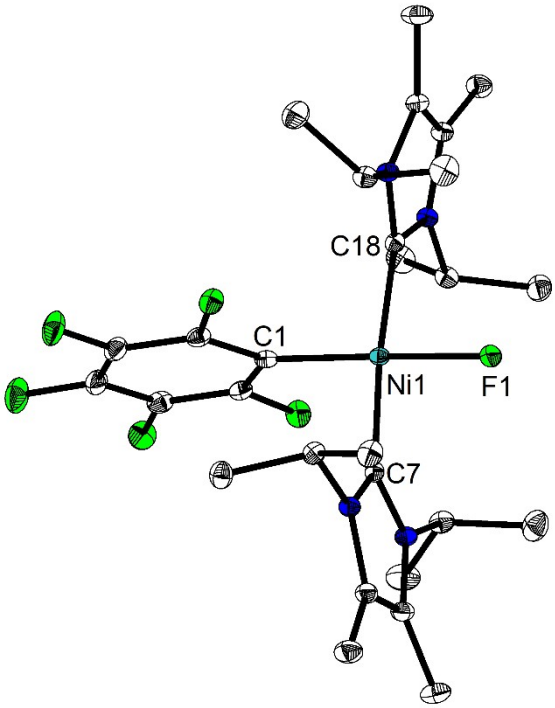

Figure S5. Molecular structure of complex **2-*i*Pr$_2$Me$_2$Im**. Thermal ellipsoids correspond to 30% probability. Hydrogen atoms as well as co-crystallised diethyl ether are omitted for clarity.

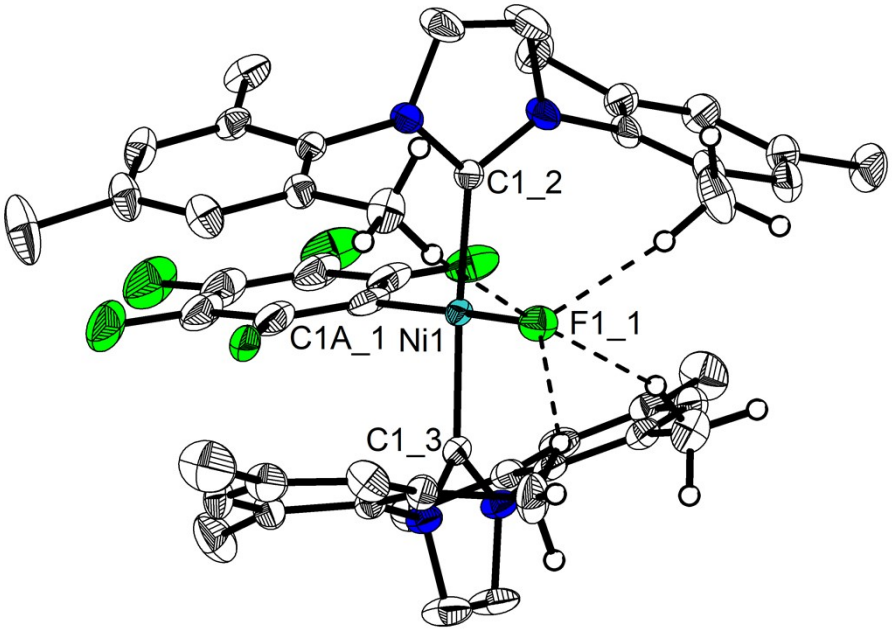

Figure S6. Molecular structure of complex **2-Mes$_2$Im**, showing weak hydrogen bonding between methyl groups and the fluoride ligand. Thermal ellipsoids correspond to 30% probability. Hydrogen atoms (except those at the CH_3 groups relevant to the hydrogen bond interaction to the Ni fluoride) are omitted for clarity. Crystallographic data of this complex were reported previously.[7]

Table S8. Analysis of the hydrogen bond interactions in complex **2-Mes$_2$Im**.

At(I)[1555.01]		At(J)	[ARU(J)]	D(I-J)	SumRad	Del	Type	X(I)	Y(I	Z(I)	X(J)	Y(J)	Z(J)	X	X - I...J
F1_1	....	H10B_2	[ ]	2.07	<< 2.67	-0.60	Intra	0.6934	0.3557	0.2735	0.7404	0.3652	0.1931	Ni1	113
F1_1	....	H19B_2	[ ]	2.31	<< 2.67	-0.36	Intra	0.6934	0.3557	0.2735	0.7488	0.4186	0.3455		
F1_1	....	H12C_3	[ ]	2.06	<< 2.67	-0.61	Intra	0.6934	0.3557	0.2735	0.7166	0.2599	0.3132	Ni1	129
F1_1	....	H19C_3	[ ]	2.46	<< 2.67	-0.21	Intra	0.6934	0.3557	0.2735	0.6397	0.2919	0.1923		

Solid-state NMR spectroscopy

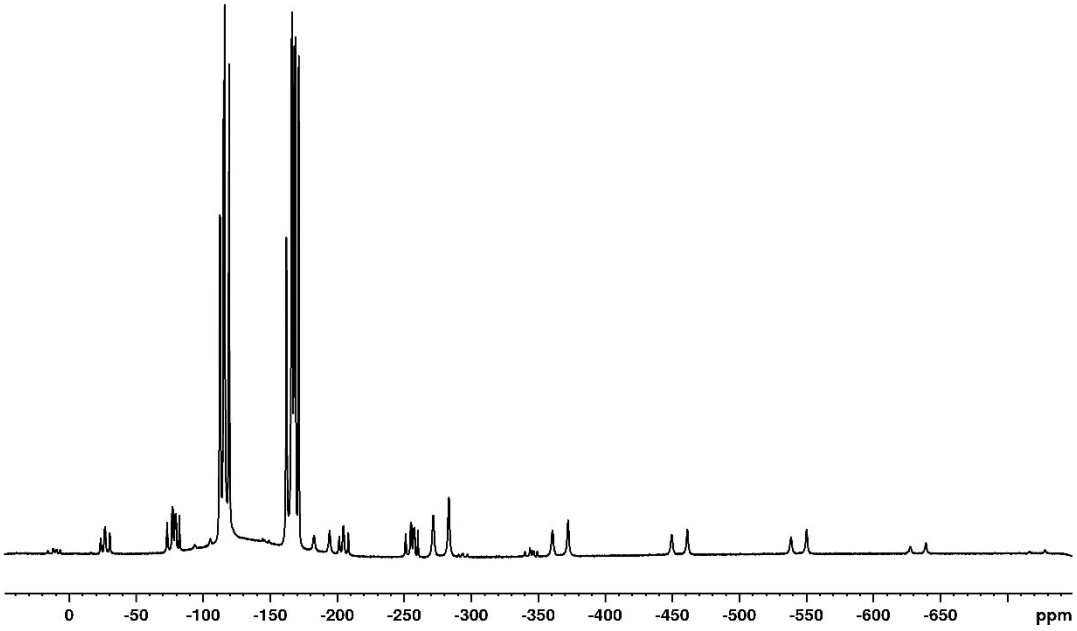

Figure S7. Experimental ^{19}F MAS SSNMR spectrum (376 MHz) of **2-*i*Pr$_2$Me$_2$Im** (spinning speed 33.5 kHz) revealing two different Ni-F signals at -360.5 ppm (δ_{11} = -77.4, δ_{22} = -303.8, δ_{33} = -700.4) and -372.2 ppm (δ_{11} = -114.3, δ_{22} = -302.3, δ_{33} = -699.9).

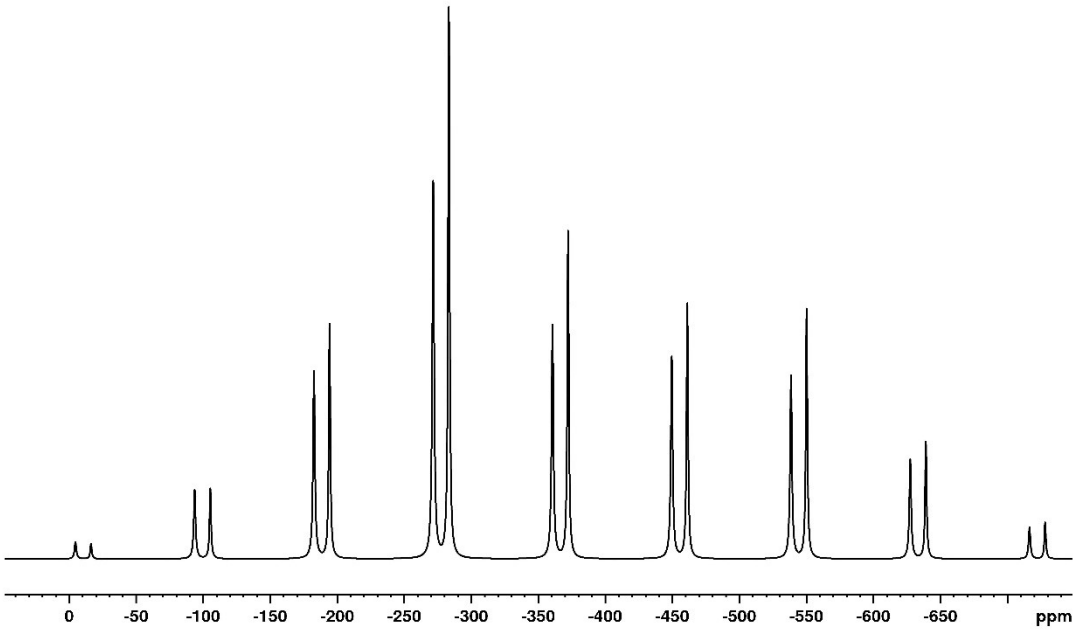

Figure S8. Best fit simulated^{19}F MAS SSNMR spectrum for the Ni-F resonances of **2-*i*Pr$_2$Me$_2$Im** (spinning speed 33.5 kHz).

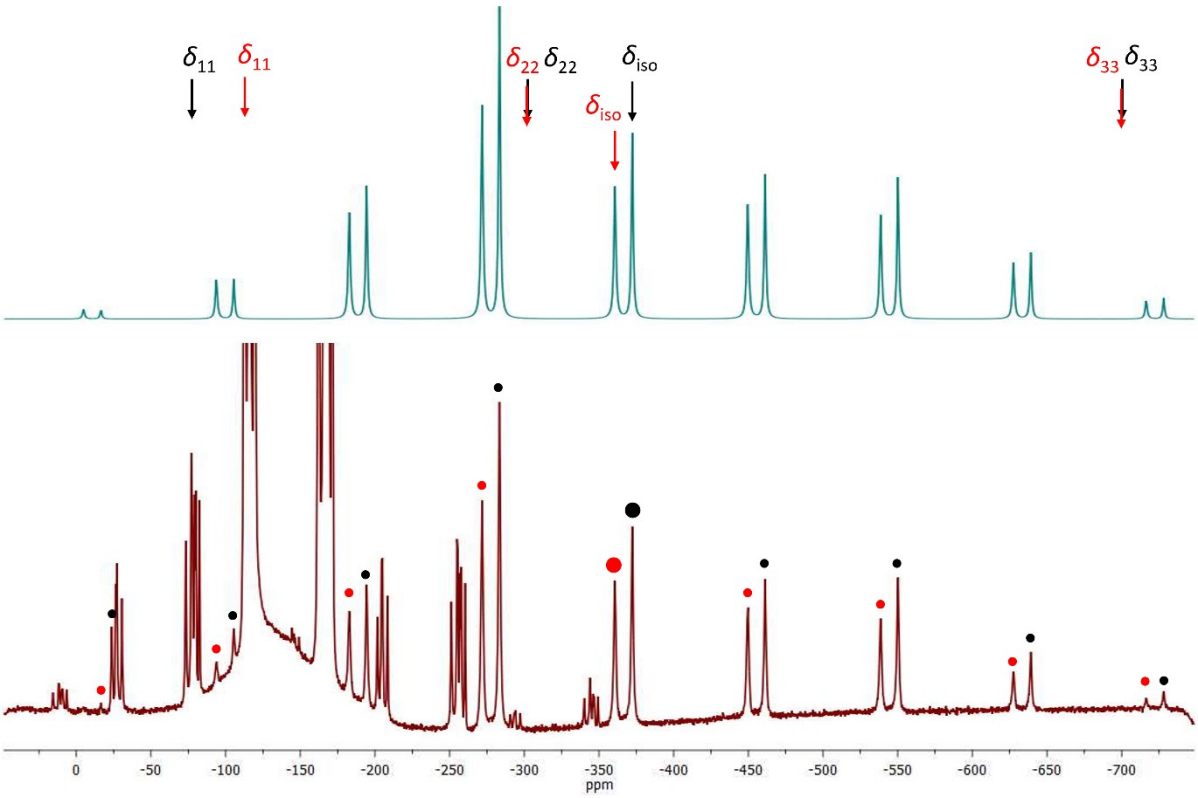

Figure S9. ^{19}F MAS SSNMR spectrum (376 MHz) of **2-*i*Pr$_2$Me$_2$Im** (spinning speed 33.5 kHz). Top: best fit simulated spectrum for the two Ni-F resonances with the positions of their shielding tensor marked. Bottom: experimental spectrum. The dots indicate the Ni-F peaks and their spinning side bands.

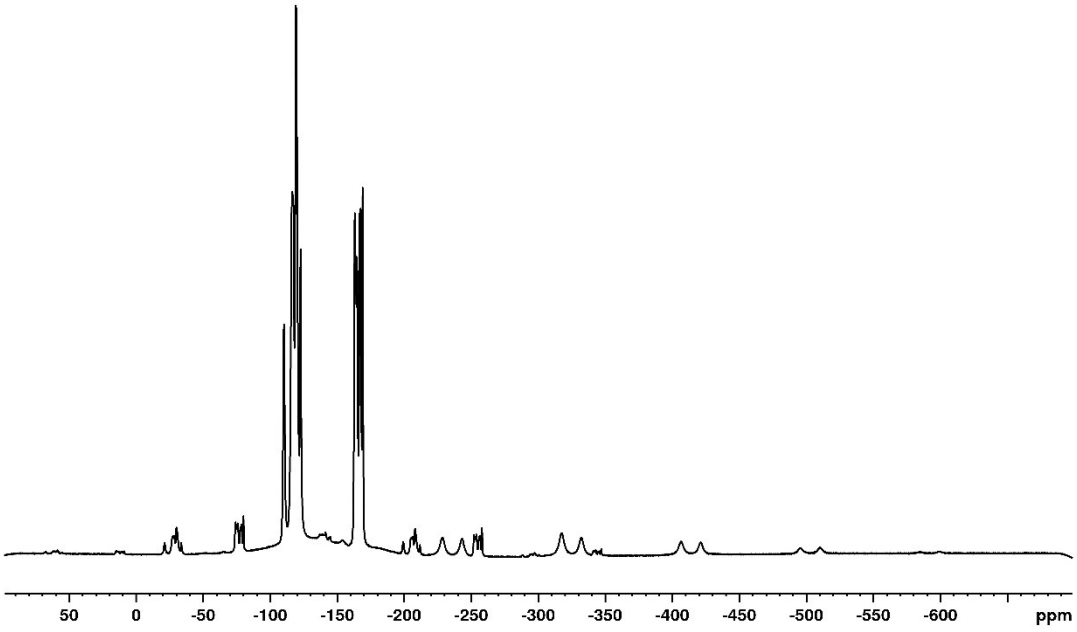

Figure S10. Experimental ^{19}F MAS SSNMR spectrum (376 MHz) of **2-*i*Pr$_2$Me$_2$Im•I-C$_6$F$_4$-I** (spinning speed 33.5 kHz) revealing two different Ni-F signals at -317.4 ppm (δ_{11} = -121.9, δ_{22} = -282.9, δ_{33} = -547.9) and -332.00 ppm (δ_{11} = -127.8, δ_{22} = -304.2, δ_{33} = -564.0).

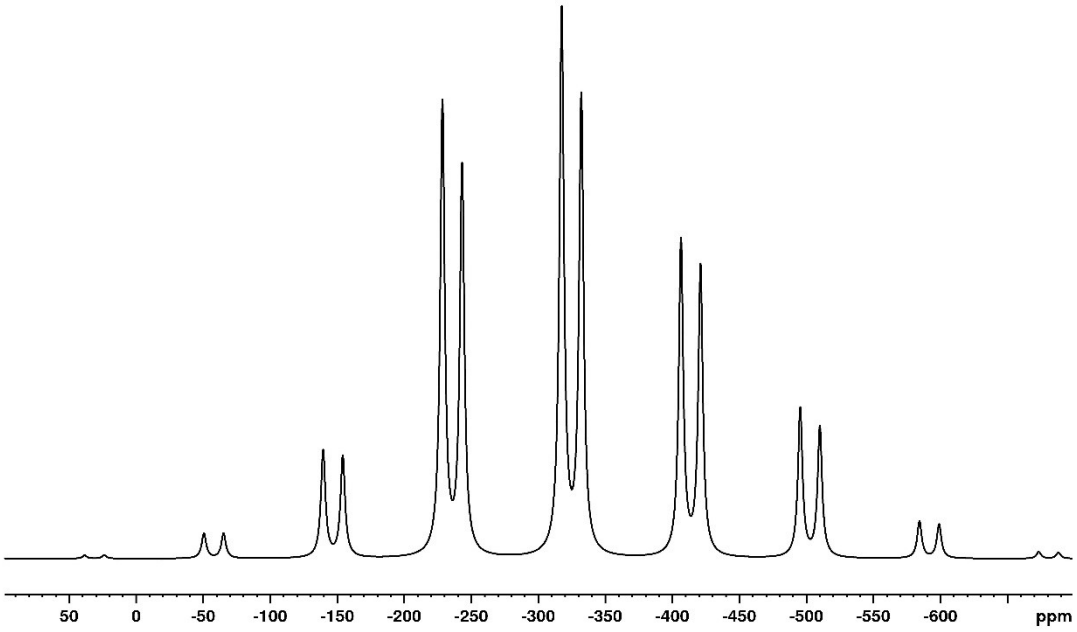

Figure S11. Best fit simulated ^{19}F MAS SSNMR spectrum for the Ni-F resonances of **2-*i*Pr$_2$Me$_2$Im•I-C$_6$F$_4$-I** (spinning speed 33.5 kHz).

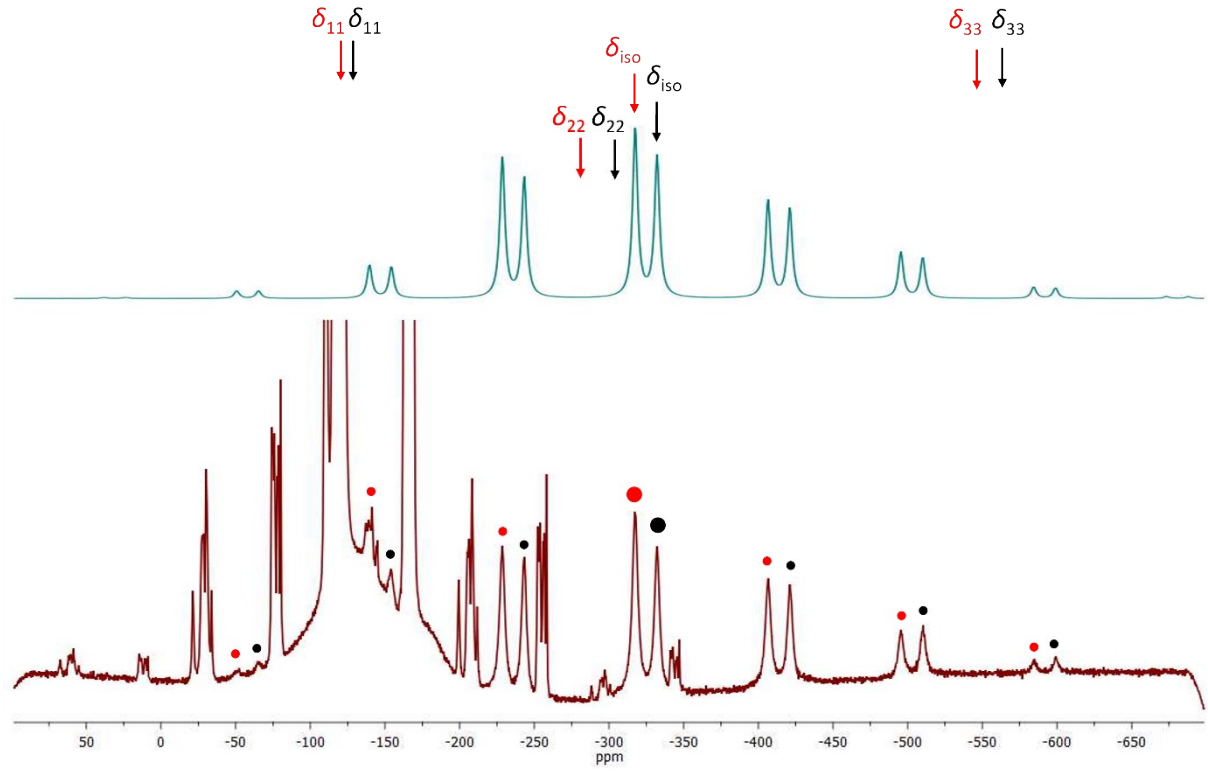

Figure S12. ^{19}F MAS SSNMR spectrum (376 MHz) of **2-*i*Pr$_2$Me$_2$Im•I-C$_6$F$_4$-I** (spinning speed 33.5 kHz). Top: best fit simulated spectrum for the two Ni-F resonances with the positions of their shielding tensor marked. Bottom: experimental spectrum. The dots indicate the Ni-F peaks and their spinning side bands.

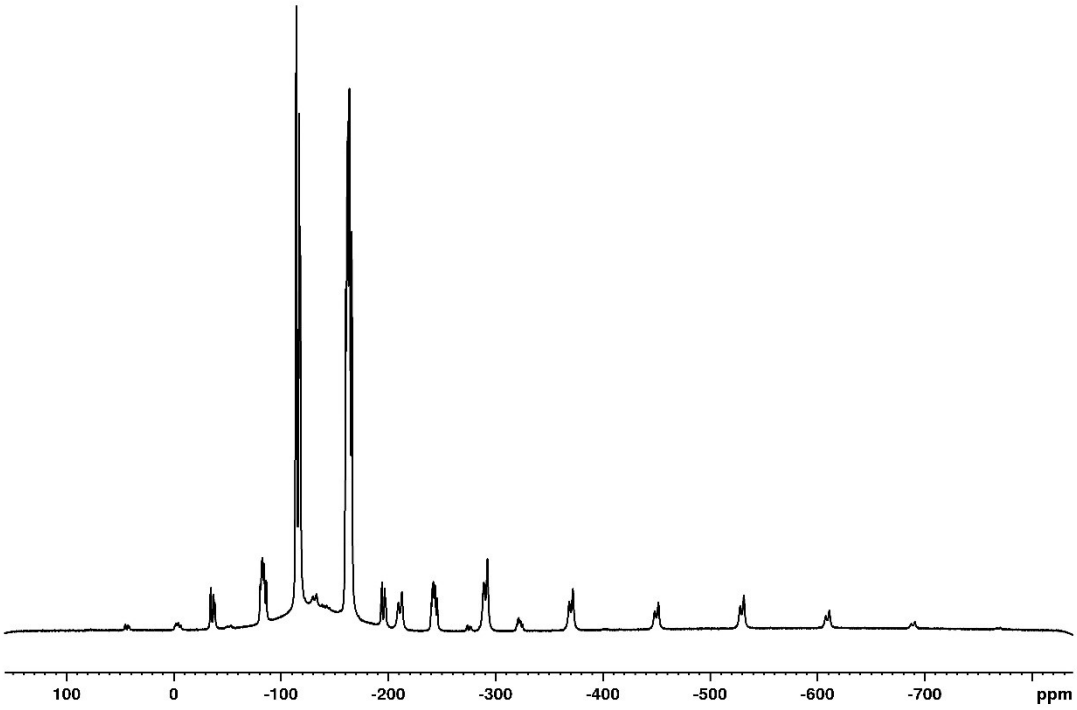

Figure S13. Experimental ^{19}F MAS SSNMR spectrum (376 MHz) of **2-*i*Pr$_2$Im** (spinning speed 30.0 kHz) revealing two different Ni-F signals at -368.2 ppm (δ_{11} = -131.9, δ_{22} = -290.9, δ_{33} = -681.7) and -371.7 ppm (δ_{11} = -143.2, δ_{22} = -287.2, δ_{33} = -684.7).

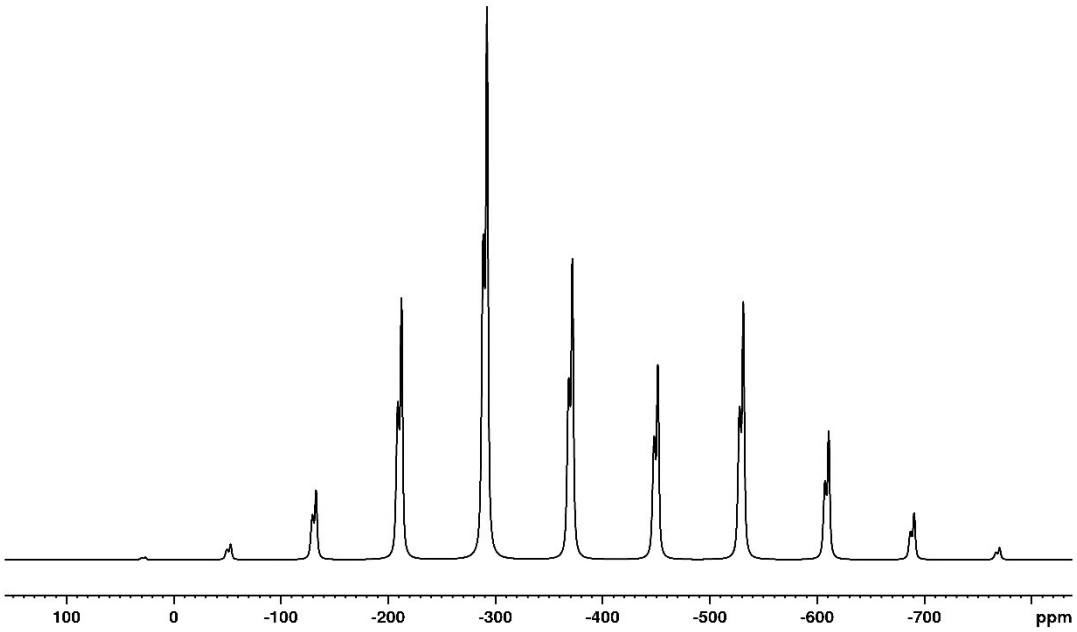

Figure S14. Best fit simulated^{19}F MAS SSNMR spectrum for the Ni-F resonances of **2-*i*Pr$_2$Im** (spinning speed 30.0 kHz).

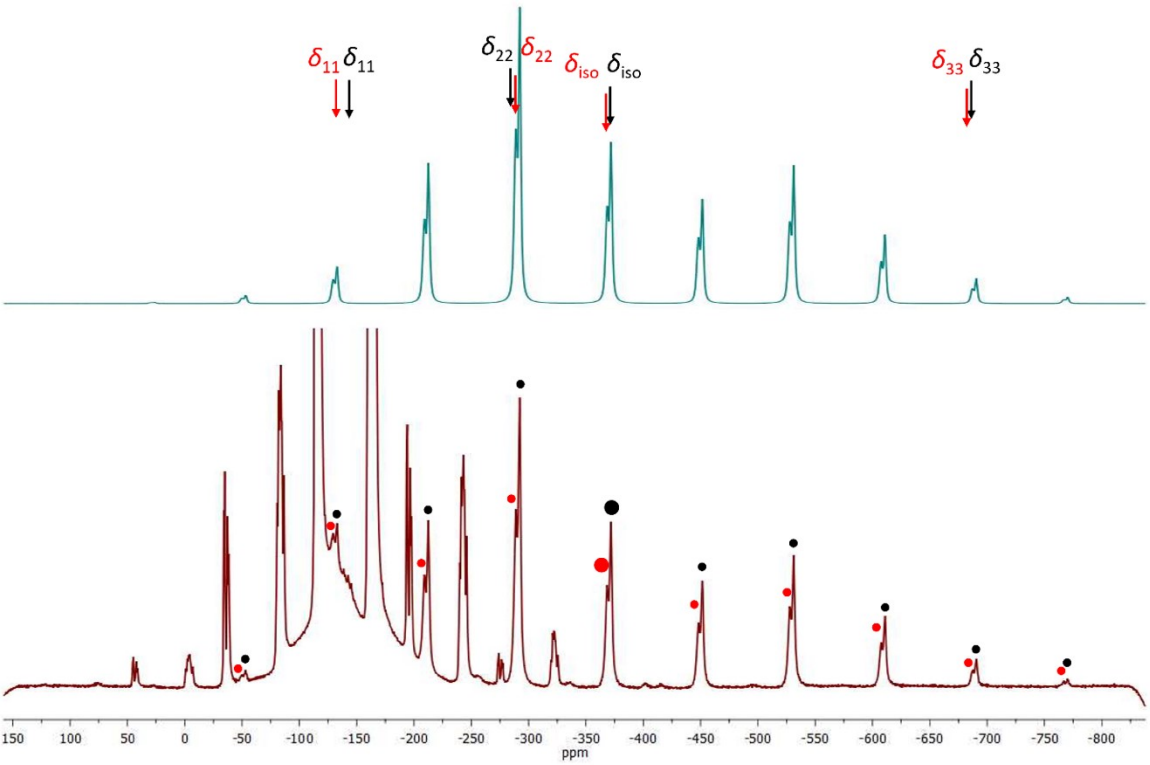

Figure S15. ^{19}F MAS SSNMR spectrum (376 MHz) of **2-*i*Pr$_2$Im** (spinning speed 30.0 KHz). Top: best fit simulated spectrum for the two Ni-F resonances with the positions of their shielding tensor marked. Bottom: experimental spectrum. The dots indicate the Ni-F peaks and their spinning side bands.

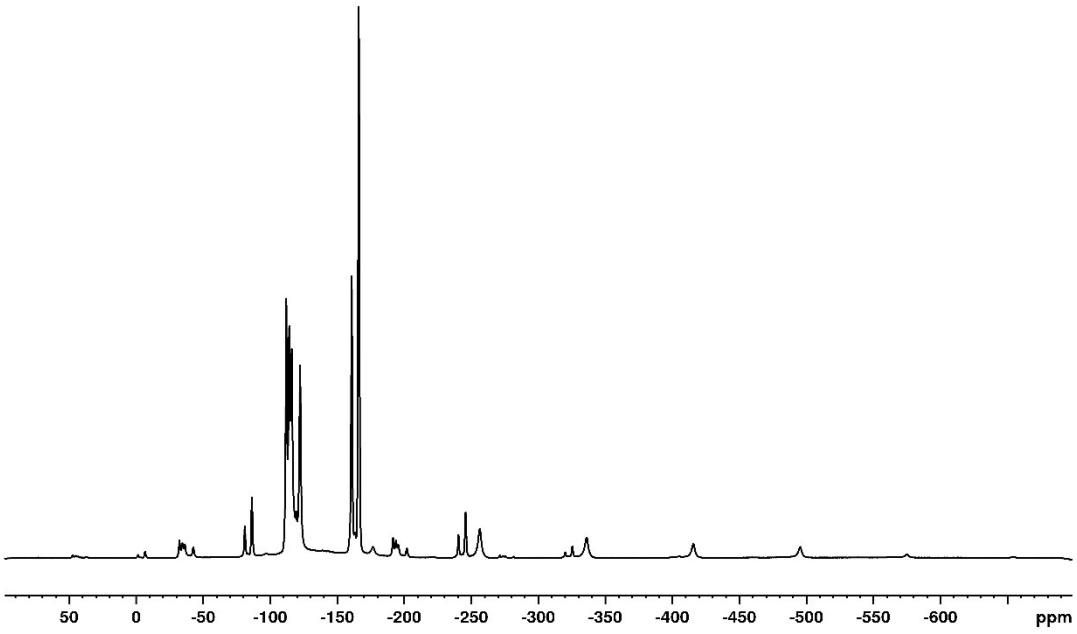

Figure S16. Experimental ^{19}F MAS SSNMR spectrum (376 MHz) of **2-*i*Pr$_2$Im•I-C$_6$F$_4$-I** (spinning speed 30.0 kHz) revealing one Ni-F signal at -335.9 ppm (δ_{11} = -145.7, δ_{22} = -276.0, δ_{33} = -586.0).

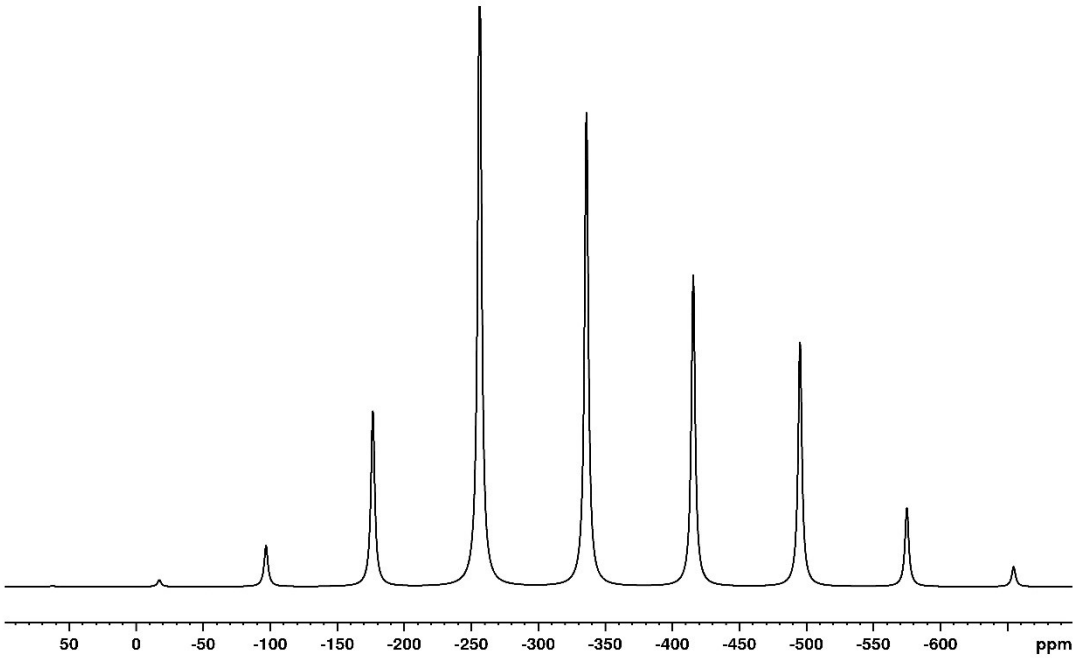

Figure S17. Best fit simulated[19]F MAS SSNMR spectrum for the Ni-F resonance of **2-*i*Pr$_2$Im•I-C$_6$F$_4$-I** (spinning speed 30.0 kHz).

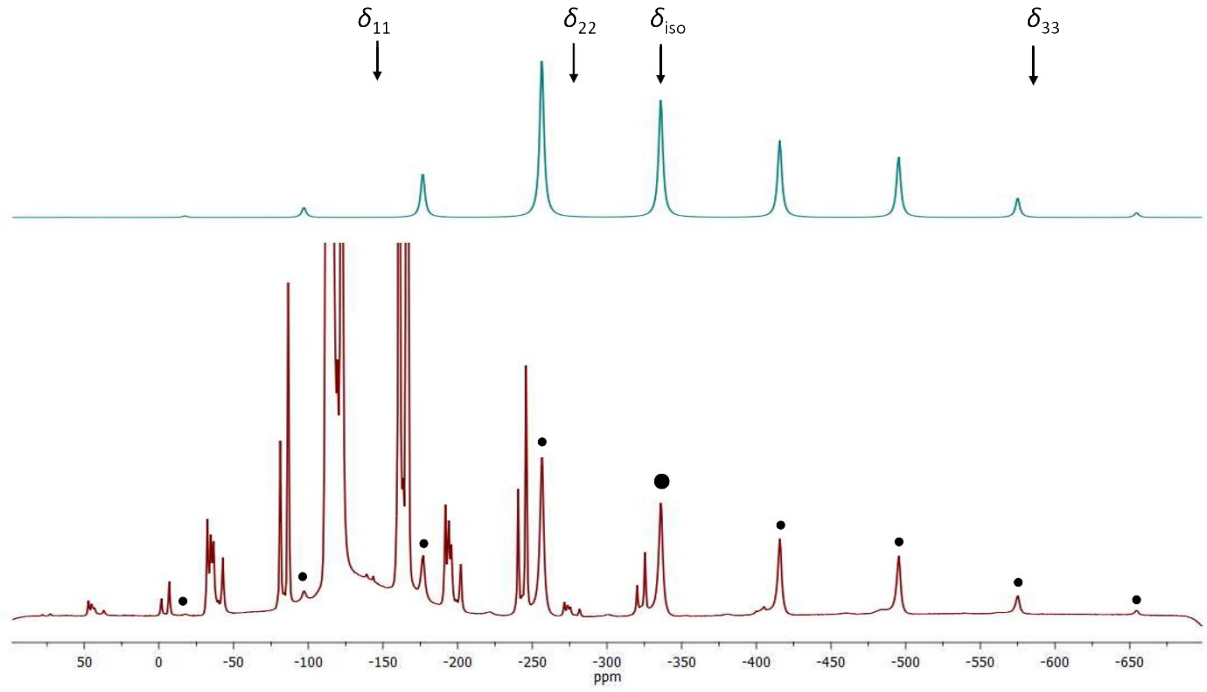

Figure S18. [19]F MAS SSNMR spectrum (376 MHz) of **2-*i*Pr$_2$Im•I-C$_6$F$_4$-I** (spinning speed 30.0 KHz). Top: best fit simulated spectrum for the Ni-F resonance with the position of the shielding tensor marked. Bottom: experimental spectrum. The dots indicate the Ni-F peak and its spinning side bands.

References

1 R. K. Harris, E. D. Becker, S. M. Cabral de Menezes, R. Goodfellow and P. Granger, *Pure Appl. Chem.,* 2001, **73,** 1795-1818.

2 G. Sheldrick, *Acta Crystallogr., Sect. A,* **2015**, *71*, 3-8

3 L. Tendera, M. Helm, M. J. Krahfuss, M. W. Kuntze-Fechner and U. Radius, *Chem. Eur. J.*, 2021, **27**, 17849-17861.

4 T. Schaub, P. Fischer, A. Steffen, T. Braun, U. Radius and A. Mix, *J. Am. Chem. Soc.*, 2008, **130**, 9304-9317.

5 a) S. Libri, N. Jasim, R. N. Perutz and L. Brammer, *J. Am. Chem. Soc.*, 2008, **130**, 7842-7844; b) T. Beweries, L. Brammer, N. A. Jasim, J. E. McGrady, R. N. Perutz and A. C. Whitwood, *J. Am. Chem. Soc.*, 2011, **133**, 14338–14348; c) M. Joksch, H. Agarwala, M. Ferro, D. Michalik, A. Spannenberg and T. Beweries, *Chem. Eur. J.*, 2020, **26**, 3571-3577.

6 C. Ammann, P. Meier and A. E. Merbach, *J. Magn. Res.*, 1982, **46**, 319-321.

7 M. W. Kuntze-Fechner, H. Verplancke, L. Tendera, M. Diefenbach, I. Krummenacher, H. Braunschweig, T. B. Marder, M. C. Holthausen and U. Radius, *Chem. Sci.*, 2020, **11**, 11009-11023.